GENERATION AND REVERSAL OF MAGNETIC DIPOLE FIELD IN 3-D MHD SIMULATION

Márcia M. Ochi, Akira Kageyama, and Tetsuya Sato

Theory and Computer Simulation Center, National Institute for Fusion Science
Toki 509-5292, Gifu, Japan

Abstract

Computer simulation results of a compressible convective magnetohydrodynamic (MHD) dynamo in a rotating spherical shell are presented. In the non-linear phase, the magnetic and kinetic energies oscillate between two fluctuating levels. The reversal of either magnetic dipole or octapole is observed at each transition between different energy levels.

1. Introduction

The magnetic field generation by convective MHD dynamo is a fascinating research topic finding many applications in planetary and solar physics. For example, it is well known that the Sun and the Earth have magnetic fields dominantly dipolar and these fields may reverse polarity. The three-dimensional, non-linear, and self-consistent nature of the dynamo problem make computer simulation a very important tool in MHD dynamo research. Recently, much computer simulation effort has been done in this research with important contributions (see [1] and references therein). The generation of magnetic dipole field in a rotating spherical shell was successfully demonstrated in our previous work [1]. The physical mechanism was interpreted as a combination of α and ω-dynamos in the mid-portion of the spherical shell. In this work we present the results of a very long simulation run of our simulation code. The two main points we would like to highlight here are (a) the observation of different regimes in the non-linear phase and (b) the dipole and octapole magnetic field reversals observed in the transition between different regimes.

2. The model

The simulation model is simple but contains the essential elements required to understand the fundamental physical processes in MHD dynamo. We study a system consisting of an inner spherical core, that has a heat source to keep its surface ($r = r_i$) at a high temperature; an outer spherical surface ($r = r_o$) that is kept at a low temperature; and an intermediate conducting fluid between these two spherical boundaries. The fluid motions are driven by thermal convection. The system rotates eastwards at a constant angular velocity Ω. We use a reference system rotating at the same angular velocity. The conducting fluid is studied by the MHD equations (including gravity and Coriolis force terms) as follows:

$$\frac{\partial \rho}{\partial t} = -\boldsymbol{\nabla}\cdot(\rho v), \tag{1}$$

$$\rho\frac{dv}{dt} = j \times B - \boldsymbol{\nabla} p + \rho g + 2\rho v \times \Omega + \mu\left(\nabla^2 v + \frac{1}{3}\boldsymbol{\nabla}(\boldsymbol{\nabla}\cdot v)\right), \tag{2}$$

$$\frac{1}{\gamma-1}\frac{dp}{dt} = -\frac{\gamma}{\gamma-1}p\boldsymbol{\nabla}\cdot v + K\nabla^2 T + \eta \boldsymbol{j}^2 + \Phi, \tag{3}$$

$$\frac{\partial A}{\partial t} = -E, \tag{4}$$

$$
\begin{aligned}
p &= \rho T, && (5)\\
B &= \boldsymbol{\nabla}\times A, && (6)\\
E &= -v\times B+\eta\boldsymbol{j}, && (7)\\
j &= \boldsymbol{\nabla}\times B, && (8)\\
\boldsymbol{\nabla}\cdot B &= 0, && (9)\\
g &= -\frac{g_0}{r^2}\hat{r}, && (10)\\
\Phi &= 2\mu\left(e_{ij}e_{ij}-\frac{1}{3}(\boldsymbol{\nabla}\cdot\boldsymbol{v})^2\right), && (11)\\
e_{ij} &= \frac{1}{2}\left(\frac{\partial v_i}{\partial x_j}+\frac{\partial v_j}{\partial x_i}\right), && (12)
\end{aligned}
$$

where ρ is the mass density, p is the pressure, v is the velocity, and B is the magnetic field. A, j, and E are the vector potential, current density, and electric field respectively. The ratio of specific heat at constant pressure to that at constant volume γ (= 5/3), the viscosity μ, the thermal conductivity K, and the electrical resistivity η are assumed to be constant. g is the gravitational acceleration, $\hat{r}$ is the radial unit vector, and g_0 is a constant.

The integration of the MHD equations in spherical coordinates (r,θ,ϕ) is based on the finite difference method. Simulations are performed in the full spherical shell region ($r_i \leq r \leq r_o, 0 \leq \theta \leq \pi, 0 \leq \phi < 2\pi$). The grid numbers ($N_r, N_\theta, N_\phi$) are chosen to be equal to (50,38,64) to achieve sufficient accuracy at reasonable CPU time. The details about the numerical techniques can be found in [2].

The boundary conditions at r_i and r_o are v= 0 and that the magnetic field has only a radial component. This guarantees that Poynting vector, $E \times B$, has no radial component on the boundaries. This ensures that any magnetic field must be a consequence of the dynamo action in the bulk of the spherical shell. The temperature on the inner boundary is 3.5 times larger than the temperature on the outer boundary. The inner and outer boundary temperatures are kept constant throughout the simulation.

The parameters for this simulation are r_i = 0.3, K = 4.243 $\times$ 10^{-3}, g_0 = 1.0, Ω = 7.0, η = 2.8 $\times$ 10^{-4}. The Taylor number is defined by T = $[2\Omega\rho(r_o - r_i)^2/\mu]^2$ and the Rayleigh number by Ra = $g_0\rho(\beta\, c_q - g_0)\,(r_o - r_i)^4/(K\,\mu)$, where β is the temperature gradient coefficient (the initial temperature profile is given by $\beta/r + const.$) and $c_q = \gamma/(\gamma-1)$. In this case, T and Ra are 5.88×10^6 and 3.36×10^4 respectively.

Lengths and temperatures are normalized to the radius r_o and the temperature on the outer boundary respectively. The normalization time is the sound crossing time (=r_o/v_s) where v_s is the sound speed. In this simulation, the thermal diffusion time and resistive diffusion time are respectively equal to 116 and 1750. The simulation goes until the time equals to 27,000, which is 15.4 times the resistive diffusion time. This simulation required approximately 300 hours of CPU time in the NEC/SX-4 supercomputer.

3. The simulation results

The simulation starts from an unstable hydrostatic and thermal equilibrium state with no mag-

netic field. A temperature perturbation is introduced which causes the convection motion to begin. After a short time (around t = 150), the system reaches the saturation energy level. At time equals to 572 a small and random magnetic field seed is introduced. Figure 1 shows the kinetic and the magnetic energies (logarithmic scale) integrated over the spherical shell versus time (normalized units). Before introducing the initial magnetic field seed and during the linear regime (from time equals to 572 until 1656), there are no fluctuations in the kinetic energy: the convection motion pattern is verified to be well-organized in five pairs of alternating cyclonic and anticyclonic convection columns whose axes are parallel to and encircle the rotation axis. The fluid in the cyclonic (anticyclonic) column rotates in the same (opposite) direction as the rotation of the spherical shell.

In the non-linear phase, when the magnetic energy becomes large, time fluctuations are observed and the average magnetic energy alternates between two fluctuating energy levels. The lower level is approximately equal to the kinetic energy, and the upper level is about five times larger. We will refer to the four different regimes in the non-linear phase as NR1, NR2, NR3, and NR4. The convection motion and the magnetic field structure are highly time dependent. Reorganization of the convection columns occurs several times during the simulation. The number of convection column pairs tends to be larger in NR2 and NR4 than in NR1 and NR3.

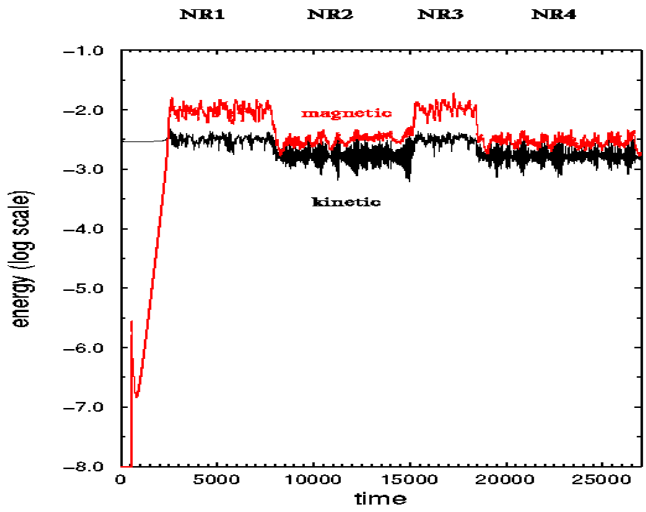

Fig. 1: It shows the magnetic and kinetic energies versus time.

The radial magnetic field on the outer boundary is expanded in spherical harmonics $Y_l^m(\theta,\phi)$, $B_r(r_o) = \sum_{l=1}\sum_{m=-l}^{l} a_l^m Y_l^m$. In Fig. 2(a), we show the dipole contribution to the total magnetic field as a function of time, which is calculated as $|a_1^0|^2/(\sum_{l=1}\sum_{m=-l}^{l}|a_l^m|^2)$. The dipole component remains as the main component during the simulation time. In Fig. 2(b), the magnitude of the dipole and the octapole moments, $|a_1^0|$ and $|a_3^0|$ respectively, versus time are presented. We can notice that the reversal of the magnetic dipole field occurs in the transition from NR1 to NR2. The octapole component reverses in the last two transitions, from NR2 to NR3 and from NR3 to NR4. In the last two transitions the dipole polarity remains the same.

From 3-D analysis, we can roughly distinguish three stages to the dipole reversal process. In the initial stage, the magnetic energy is about five times larger than the kinetic energy, and the

convection pattern consists of six straight cyclonic and anticyclonic vortex column pairs aligned to the rotation axis. In the intermediate stage, the magnetic energy decreases and the magnetic field is observed to change direction in some regions, accompanied by reorganization of the vortex columns. In the final stage, the field is completely reversed, the number of convection columns is increased and the magnetic energy is lower than in the second stage.

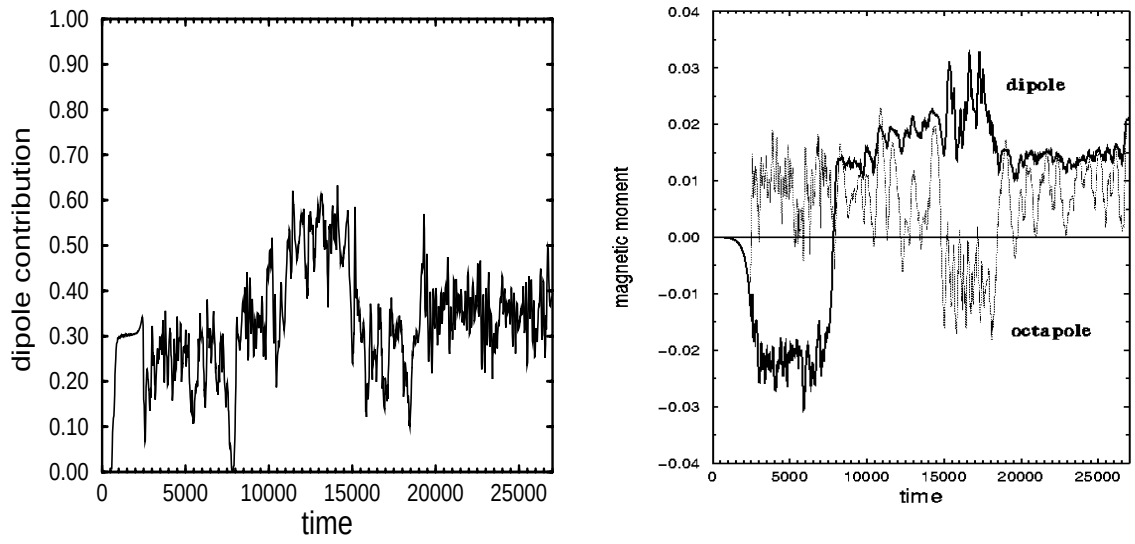

Fig. 2:(a) The dipole contribution to the total magnetic field and (b) the dipole and octapole moments versus time.

4. Summary

We presented the simulation results of a MHD dynamo driven by thermal convection in a rotating spherical shell. The results showed that a strong magnetic field was generated, preferentially the dipole. The non-linear phase was characterized by presenting different magnetic energy levels. To our knowledge, this is a new result for this kind of simulation. The transition between NR1 and NR2 was verified to be accompanied by the dipole field reversal. The other two transitions were not observed to be related to the dipole reversal, but rather to the increase or reduction in the dipole moment, as well as to the reversal of the second main symmetric mode, the octapole. These fundamental features of our simulation are to some extent in qualitative agreement with the geomagnetic data on dipole field amplitude record [3].

The reversal process does not occur at once but occurs in steps. Some of the concentration regions reverse direction first and then the other ones until the process is completed. The physical mechanism of the dipole reversal is still under investigation.

References

[1] A. Kageyama and T. Sato: Phys. Rev. E **55**, 4617 (1997).
[2] A. Kageyama and T. Sato: Phys. Plasmas **2**, 1421 (1995).
[3] J.-P. Valet and L. Meynadier: Nature **366**, 234 (1993).